Electrochemical Imaging

DOI: 10.1002/anie.201201602

# Local Redox-Cycling-Based Electrochemical Chip Device with Deep Microwells for Evaluation of Embryoid Bodies**

*Kosuke Ino,* Taku Nishijo, Toshiharu Arai, Yusuke Kanno, Yasufumi Takahashi, Hitoshi Shiku, and Tomokazu Matsue**

Three-dimensional (3D) cell cultures are important for applications in modern cell biology and tissue engineering, because these cell cultures offer architectural microenvironments very close to those of natural tissues, compared to conventional two-dimensional cultures. The environment of 3D cultures has an important effect on cell biology, including differentiation of stem cells. For example, embryonic stem (ES) cells, which can differentiate into any body organ tissues and are expected to have significant potential as cell sources for regenerative medicine, can develop into cardiomyocytes by forming 3D organ tissues, such as embryoid bodies (EBs).[1] Several biomarkers, such as alkaline phosphatase (ALP) that express undifferentiated ES cells, are used to check the differentiation level of ES cells.[2] Several types of cell arrays have recently been developed for high-throughput cell assays on cell activity and differentiation. Although fluorescence detection has been performed with cell arrays, because its sensitivity is high, the fluorescent detection has some disadvantages as described in the Supporting Information. As an alternative method, electrochemical detection has been incorporated into biosensor devices. Since electrochemical techniques have many advantages, several kinds of microelectrode arrays have been proposed and applied to chemical and biological analyses including cell arrays.[3–5] However, it is difficult to collect electrochemical responses at many individual measurement points using conventional electrochemical devices, because sufficient space for the bond pads is not available on the chip border. To solve this problem, we have proposed a novel method to realize individually addressable electrochemical measurements using a device consisting of two sets of microelectrode arrays to induce local redox cycling,[6–10] and we have designated the novel methodology as local redox cycling-based electrochemical (LRC-EC) detection. In the system, two arrays of band microelectrodes are orthogonally set to form an $n \times n$ array of crossing points with only $2n$ bonding pads for external connection. By setting the potentials at the row and column electrodes to appropriate values and inducing local redox cycling at a particular crossing point, the local redox cycling-based signals can be acquired from an individual crossing point. The detection system has been applied for the expression of reporter proteins in a cell culture array.[7,8] In addition, we have developed the LRC-EC chip device with a comb-type interdigitated array (IDA) electrode that has an open space on the sensor to introduce and collect samples with ease.[6]

In this study, the LRC-EC device was applied to evaluate EBs through their ALP activity as the marker for the cell activity and differentiation, without labeling the EBs. Deep microwells were incorporated into the chip device for trapping of EBs. The general architecture is displayed in Figure 1 A and our previous report.[6] The LRC-EC device consists of 16 row, 16 column electrodes, and 32 connector pads. The measurement procedure is illustrated in Figure 1 B and Figure S1 in the Supporting Information. The EBs are introduced into the device to trap a single EB in a microwell. Each microwell has IDA electrodes for electrochemical sensing. The EB activity is then electrochemically detected by the LRC-EC device. For imaging, the electrochemical responses at the 256 sensor microwells are collected by sequentially changing the potential applied to the row and column electrodes. After imaging, the specific EBs were collected using a capillary.

Prior to fabrication of the device, a diffusion simulation of a redox compound in the LRC-EC device was conducted and electrochemical signals in the deep microwells were calculated based on electrochemical responses to clarify the collection efficiency (CE), the number of redox cycles (RC), the cross-talk, and the time to reach steady-state. Three models were created (Figure 2 A) and the simulation was performed as detailed in Figure S2 in the Supporting Information. In dual mode (redox cycling), the current signals reach steady-state within 2 s because of the rapid formation of a steady-state diffusion layer. In single mode (no redox cycling), a long time (180 s) is necessary to attain the steady-state (Figure 2 B,C). The CEs for models 1, 2, and 3 were 46.9, 74.3, and 82.8 %, respectively (Table S1 in the Supporting Information). The CE value approached 100 % as the electrode gap was reduced. As the height of the microwells

[*] Dr. K. Ino, T. Nishijo, T. Arai, Y. Kanno, Dr. H. Shiku, Prof. Dr. T. Matsue
Graduate School of Environmental Studies, Tohoku University
Sendai (Japan)
E-mail: ino.kosuke@bioinfo.che.tohoku.ac.jp
matsue@bioinfo.che.tohoku.ac.jp
Dr. Y. Takahashi, Prof. Dr. T. Matsue
Advanced Institute for Materials Research, Tohoku University
Sendai 980-8579 (Japan)

[**] This work was supported in part by the Japan Society for the Promotion of Science (JSPS) with Grants-in-Aid for Scientific Research (A, grant number 22245011) and for Young Scientists (B, grant number 23760745). This study was also supported by the Asahi Glass Foundation and the Mitsui Sumitomo Insurance Welfare Foundation. This work was partly supported by the Cabinet Office, Government of Japan, through its "Funding Program for Next Generation World-Leading Researchers".

Supporting information for this article is available on the WWW under http://dx.doi.org/10.1002/anie.201201602.

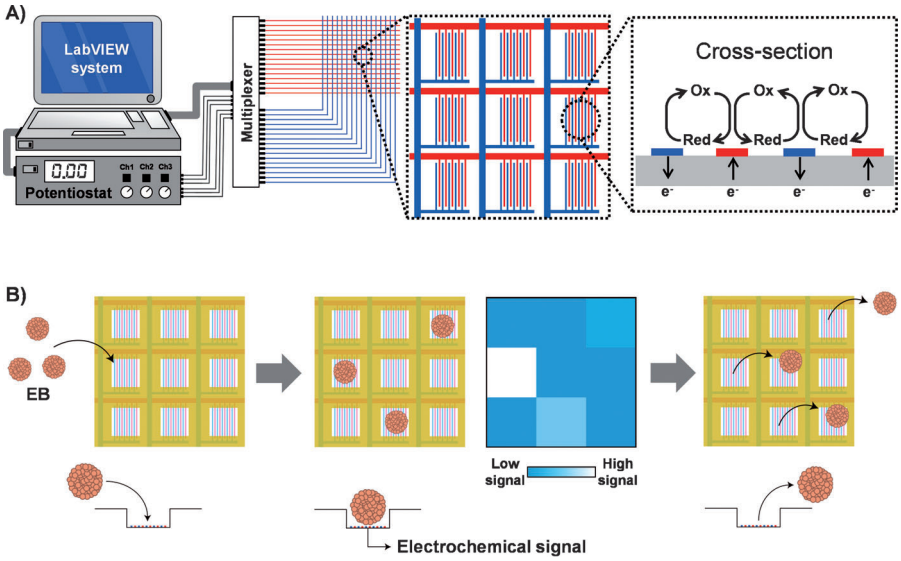


***Figure 1.*** Detection of EBs using the LRC-EC device. A) The LRC-EC device consists of 16 row and 16 column electrodes. The potentiostat is connected to these electrodes through the multiplexer, and the instruments are controlled with a computer. Local redox cycling is induced only at the IDAs located at the designated cross-points. B) The EBs are introduced into the device and after the EBs are trapped into the microwells, the electrochemical signals from the EBs are acquired and the EBs are then collected. The detection scheme for ALP on EBs is shown in Figure S1 in the Supporting Information.

increased from 7 to 50 μm, the current response in single mode was reduced from 6.25 to 4.93 nA, because deep microwells prevent the diffusion of redox species from the bulk to the electrode. Although deep microwells are necessary for trapping 3D culture cells, they have a disadvantage in that they affect the sensitivity in single mode. In contrast, the collector (reduction) current in dual mode increased from 52.7 to 55.5 nA and the CE increased from 74.3 to 82.8%, because the chance of redox species diffusing into the bulk of the solution was significantly reduced by the walls of the microwells (Table S1 in the Supporting Information). In addition, the number of RCs increased from 11.4 to 13.6 (Table S1). As the width of the electrodes and the gap between the electrodes was reduced, the time to reach steady-state in dual mode was reduced (Figure 2D). These results indicate that the total scanning time can be shortened by reducing the width of the electrode and the gap between the electrodes.

In assays using an electrode array, cross-talk caused by diffusion of redox compounds formed in neighboring electrodes during detection induces artifacts in the electrochemical signals and imaging data. When the distance between sensors is close, electrochemical cross-talk becomes a serious issue, because the diffusion layer overlaps during detection. Figure 2E shows the concentration profile of the species formed at the electrode after reaching steady-state (single mode: 180 s, dual mode: 2 s) for model 3. In dual mode measurements, there is no obvious overlap of diffusion layers between the neighboring sensors, because the wall is sufficiently high to block the diffusion; therefore, the undesired influence of cross-talk is negligible. On the contrary, cross-talk becomes a serious problem in single mode measurements in the steady-state. These results show that an LRC-EC system based on dual mode measurements is useful for electrochemical array detection, because of rapid detection and the lack of cross-talk, the latter of which is advantageous for further miniaturization of the array.

Based on the simulation results, an LRC-EC device was fabricated that consisted of IDA electrodes (10 fingers, 5 μm wide, 5 μm gap) and deep microwells (50 μm depth). The fabrication process for the LRC-EC device is schematically illustrated in Figure S3 in the Supporting Information. Over 250 sensors were incorporated into a single chip with only 32 connector pads (Figure S4 in the Supporting Information). The present LRC-EC device has an open space and deep microwells to easily accommodate and release the cell aggregates (Figure 1). It should be noted here that a high density of sensor points can be achieved in the LRC-EC device, whereas the integration of a large number of electrodes is difficult in a conventional array device, because of limited space for connecting lines and bond pads in the device (Figure S5 in the Supporting Information).

The electrochemical performance of the LRC-EC device was investigated using *p*-aminophenol (PAP), a redox compound that shows reversible electrochemical behavior and a product of ALP-catalyzed reaction (Figure S1A in the Supporting Information). The CE and RC were calculated from the experimental results (Figure 3 and Figure S6 in the Supporting Information). Steady-state generator and collector currents were detected within a few seconds after the potential step in dual mode. For comparison, in single mode, the steady-state current was observed more than 100 seconds after the potential step. Therefore, the LRC-EC device is effective for rapid electrochemical imaging when operated in dual mode. The collector current per sensor in a 1.0 mM PAP solution in dual mode was 42.5 nA, which was 17.2 times larger than the oxidation current per microwell in single mode under the same conditions. These results indicate effective signal amplification by redox cycling in the LRC-EC device. The device consisted of deep microwells and the IDA electrode, so that the CE was also high (87.8%). These experimental currents were lower than the simulation results (Figure 3 and Table S1), probably because of electrode fouling during redox cycling.[11] No charging current was observed at the collector in dual mode, because the potential of the collector was fixed, which enabled a rapid scanning process, whereas a significant charging current was observed in single mode (Figure 3). The electrochemical signals at the individual sensors were proportional to the concentration of PAP and the detection limit was found to be less than 1 μM.

  

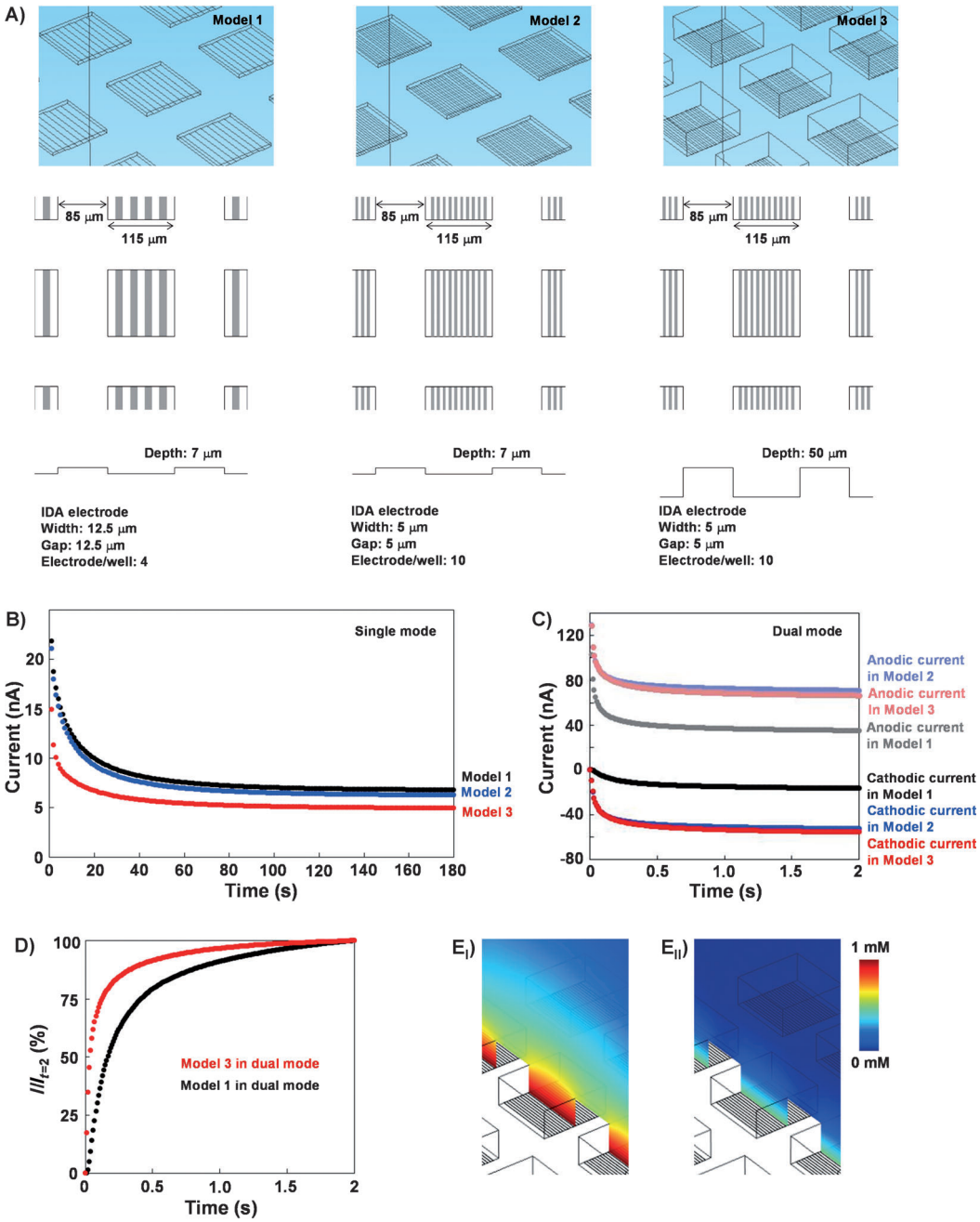


***Figure 2.*** Current simulation for redox compound diffusion using simulation software. A) Model images, where the microwells were placed on the bottoms of the models and the band electrodes were placed on the bottoms of the microwells. B–D) Amperograms of 1.0 mM redox species constructed by calculating redox currents. Currents at the anode and cathode electrodes in models 1, 2, and 3 in B) single mode and C) dual mode. Detailed information is provided in Figure S2 in the Supporting Information. D) Time-course analysis of a cathodic current on a steady-state current. The percentage in the graph was calculated by dividing the current by that obtained after 2 s. E) Cross-sectional images on the oxidants after reaching the steady-state current in single ($E_I$, after 180 s) and dual modes ($E_{II}$, after 2 s).

Thus, the present LRC-EC device can be used for quantitative determination of PAP (Figure 3C). The LRC-EC device can also be applied to detect neurotransmitters such as dopamine, a redox compound showing reversible electrochemical behavior. The sensitivity of the LRC-EC device will further be improved by incorporating nanogap electrodes which enhance the efficiency of redox cycling.[12] We now plan to fabricate a nanogap LRC-EC to detect trace amount of redox species. Electrochemical imaging with LRC-EC was conducted using only the collector current, because the collector current does not contain the undesired influence of charging currents.

The detection of PAP with LRC-EC was applied to characterize EB activity using ALP as a marker, as described in Figure S1. Mouse ES cells (129/Sv) were cultured and EBs were formed by the hanging drop method as described in the Supporting Information. After EB formation, the EBs were collected with a glass capillary and introduced onto the LRC-EC device. As a preliminary experiment, a large EB was introduced on the LRC-EC device, and electrochemical images were acquired every 0.5 min (Figure 4A). The electrochemical images consisted of 256 pixels with background-corrected currents. The image shows that the EB size was approximately 600 μm in diameter, which was similar to that observed by conventional optical imaging. The current signal originates from the redox cycling of PAP generated by the ALP-catalyzed reaction at EBs; therefore, the image does not directly reflect the size of the EB. The EB image becomes broad because the PAP diffuses to the neighboring sensors (Figure 4 $A_{III}$).

Cross-talk because of enzymatic products can be avoided by confining an EB in a single microwell with tall walls. Single

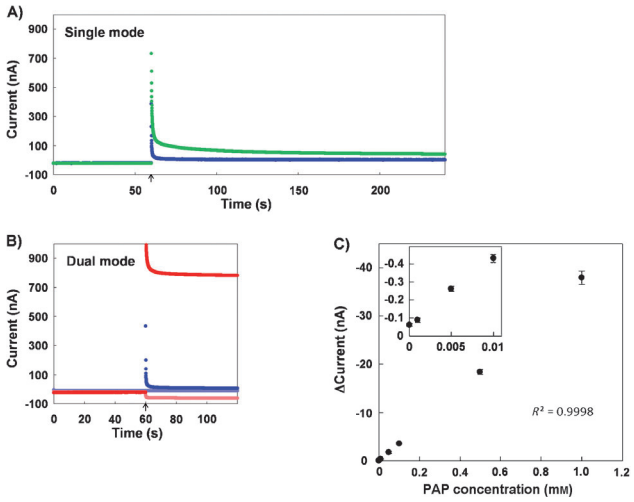


***Figure 3.*** Evaluation of the LRC device performance. Amperograms for 0 and 1.0 mM PAP in A) single and B) dual modes. In single mode, all electrodes were stepped from −0.30 to 0.30 V at the time indicated by the arrow and responses were acquired without PAP solution (blue) and with 1.0 mM PAP solution (green). In dual mode, the column electrode was stepped from −0.30 to 0.30 V at the time indicated by the arrow, while the other electrodes were held at −0.30 V, as shown in Figure S6 in the Supporting Information. Responses from the PAP solution at the column electrode (0 mM: blue; 1 mM: red) and the row electrode (0 mM: aqua; 1 mM: pink). C) Dependence of the electrochemical signals on the PAP concentration (0.001–1 mM). The signal was detected at the row electrodes 2 s after the potential step of the column electrode from −0.30 to 0.30 V. The signal before the potential step (background) was subtracted from the signal after 2 s of the potential step. Data points represent mean values (±standard deviation) of five independent experiments.

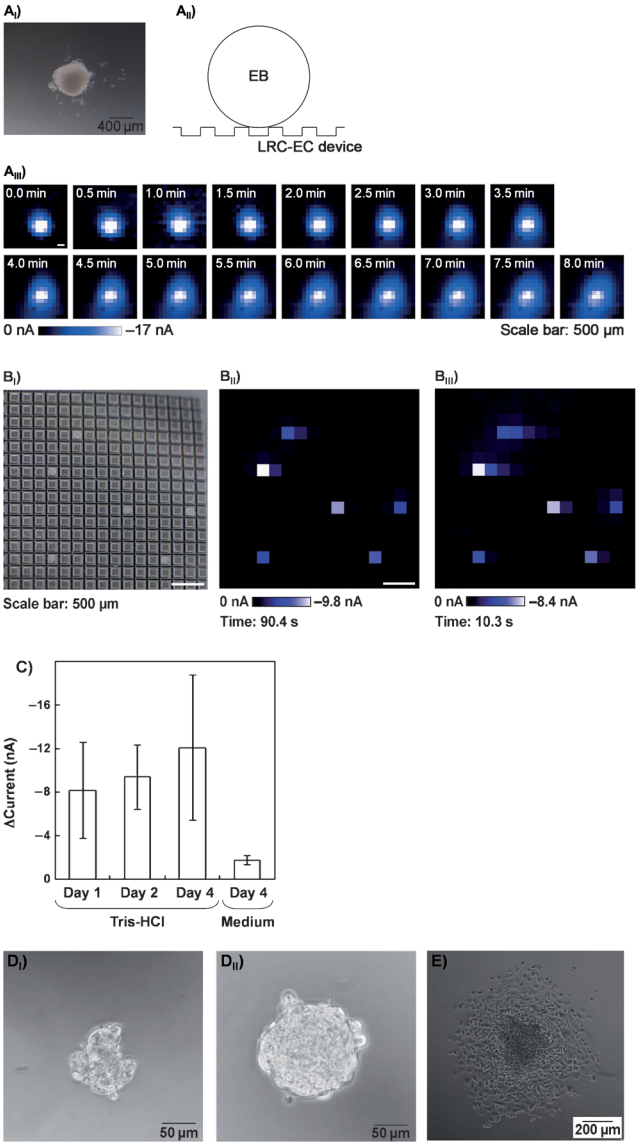


***Figure 4.*** Electrochemical imaging of the EBs. Hanging droplets (1000 cells, 20 μL) were incubated for 6 days and the large EBs were then electrochemically detected ($A_I$: optical image; $A_{II}$: detection image; $A_{III}$: time-course electrochemical image). Hanging droplets (150 cells, 20 μL) were incubated for 4 days and the small EBs were then electrochemically detected ($B_I$: optical image; $B_{II}$ and $B_{III}$: electrochemical image). The scanning times for acquiring one electrochemical image were 90.4 s ($B_{II}$) and 10.3 s ($B_{III}$), respectively. Hanging droplets (150 cells, 20 μL) were incubated for 1–4 days to detect the EBs. C) Day 1: $N=8$; Day 2: $N=6$; Day 4: $N=19$; Day 4: Medium, $N=4$. Tris-HCl or culture medium containing 4.7 mM PAPP was used as a substrate to investigate the effect of buffer on the electrochemical signal. Optical images of the EBs were acquired after culturing for 1 day ($D_I$) and 4 days ($D_{II}$). After the EBs cultured for 4 days were electrochemically detected in the culture medium, the EBs were collected and cultured on a gelatin-coated dish for 2 days (E).

EBs were placed into designated single microwells with 50 μm walls. Figure 4B shows that the image followed the position of the EBs on the device. The EB fitted the microwell size, so that the signal was only acquired from sensor microwells where the EBs were trapped. The tall walled microwells were useful to prevent the redox compounds from diffusing toward neighboring microwells, which resulted in the acquisition of a clear electrochemical image. It is also important to reduce the time to reach steady-state for rapid acquisition of electrochemical signals from sensor microwells. An electrochemical image consisting of 256 pixels was acquired in 10.3 s by applying fast scanning detection (0.64 s per row), although the electrochemical image was less clear than that by slow scanning detection (90.4 s per image; Figure 4 $B_{III}$). The imaging time can be further shortened by using a device with narrow IDA electrode gaps. These results demonstrate that the LRC-EC device can be applied for real-time monitoring of 3D culture cells.

The EBs cultured for 1, 2, and 4 days were detected on the LR-EC device (Figure 4C). The electrochemical signals due to ALP activity of the EBs increased with the culture period (Figure 4C). However, the electrochemical signal did not increase as expected from the increase in the size of the EBs (Figure 4 $D_I$ and $D_{II}$), which indicates that the ALP activity per cell may be reduced and the EBs may be differentiated during culture. A culture medium (pH 7.4) containing PAPP was also used for electrochemical measurements. Under these conditions, the electrochemical signal was reduced (Figure 4C), because ALP shows lower activity in neutral pH values compared with the optimal pH 9.5. Although the signals were lowered, the collected EBs were cultured

  

successfully after electrochemical detection (Figure 4E). Therefore, we propose that the LRC-EC device is useful for high-throughput cell screening. Although the standard deviation in Figure 4C was very large, the results also showed that the differentiation level of the EBs varied considerably even if the culture period was the same because the EBs were formed from a small amount of ES cells that have heterogeneities. Therefore, it is necessary to sort EBs for quality-controlled differentiation induction culture. Since the present LRC-EC device can be used to evaluate EBs through their ALP activity and the designated EBs can be collected, the LRC-EC device will be useful to sort EBs. This strategy is much reliable and effective compared to conventional morphological observations with optical method.

In conclusion, deep microwells were incorporated into an LRC-EC device to trap single 3D culture cells and evaluate the cell activity. Simulations and the corresponding experiments were carried out to clarify the effect of the deep microwells on the LRC-EC system. Simulations using microwell models demonstrated that deep microwell arrays and fine IDA electrodes for electrochemical detection result in a high sensitivity and low cross-talk influence compared with conventional devices that employ electrode arrays for comprehensive detection. The time to reach steady-state was short, so that an electrochemical image consisting of 256 pixels was acquired in 10.3 s using the LRC-EC device. In this study, the LRC-EC device was applied to evaluate EBs through their ALP activity and the ALP activity on the EBs was successfully detected. Furthermore, the collected EBs were successfully cultured. These results indicate that an LRC-EC chip device with deep microwells is useful for the evaluation of 3D organ tissues.

Received: February 28, 2012
Revised: April 26, 2012
Published online: May 25, 2012

**Keywords:** cell analysis · cell biology · electrochemistry · microelectrodes

[1] J. Park, C. H. Cho, N. Parashurama, Y. Li, F. Berthiaume, M. Toner, A. W. Tilles, M. L. Yarmush, *Lab Chip* **2007**, *7*, 1018–1028.
[2] K. Guan, J. Rohwedel, A. M. Wobus, *Cytotechnology* **1999**, *30*, 211–226.
[3] M. Pedrero, S. Campuzano, J. M. Pingarrón, *Sensors* **2009**, *9*, 5503–5520.
[4] X. Xu, S. Zhang, H. Chen, J. Kong, *Talanta* **2009**, *80*, 8–18.
[5] K. C. Cheung, P. Renaud, H. Tanila, K. Djupsund, *Biosens. Bioelectron.* **2007**, *22*, 1783–1790.
[6] K. Ino, W. Saito, M. Koide, T. Umemura, H. Shiku, T. Matsue, *Lab Chip* **2011**, *11*, 385–388.
[7] M. Takeda, H. Shiku, K. Ino, T. Matsue, *Analyst* **2011**, *136*, 4991–4996.
[8] Z. Lin, Y. Takahashi, T. Murata, M. Takeda, K. Ino, H. Shiku, T. Matsue, *Angew. Chem.* **2009**, *121*, 2078–2080; *Angew. Chem. Int. Ed.* **2009**, *48*, 2044–2046.
[9] Z. Lin, Y. Takahashi, Y. Kitagawa, T. Umemura, H. Shiku, T. Matsue, *Anal. Chem.* **2008**, *80*, 6830–6833.
[10] X. Zhu, K. Ino, Z. Lin, H. Shiku, G. Chen, T. Matsue, *Sens. Actuators B* **2011**, *160*, 923–928.
[11] A. Walter, J. Wu, G. U. Flechsig, D. A. Haake, J. Wang, *Anal. Chim. Acta* **2011**, *689*, 29–33.
[12] B. Wolfrum, M. Zevenbergen, S. Lemay, *Anal. Chem.* **2008**, *80*, 972–977.

  